DETERMINATION OF THE ANALYTICAL WORKSPACE BOUNDARIES OF A NOVEL 2-DOF PLANAR TENSEGRITY MECHANISM

Marc Arsenault
Department of Mechanical Engineering, Royal Military College of Canada, Kingston, Ontario, Canada
E-mail: marc.arsenault@rmc.ca

Received December 2009, Accepted December 2009
No. 09-CSME-32, E.I.C. Accession 3118

ABSTRACT

Tensegrity mechanisms are slowly emerging as potential alternatives to more conventional mechanisms for certain types of applications where a reduced inertia of the mobile parts and a high payload to weight ratio are sought. With this in mind, a two-degree-of-freedom planar tensegrity mechanism is developed using a simple actuation strategy to keep the mechanism in self-stressed configurations. Solutions to the mechanism's direct and inverse kinematic problems are first developed and are then used to determine analytical expressions for its workspace boundaries.

DÉTERMINATION DES FRONTIÈRES DE L'ESPACE ATTEIGNABLE SOUS FORME ANALYTIQUE POUR UN NOUVEAU MÉCANISME DE TENSÉGRITÉ PLAN À DEUX DEGRÉS DE LIBERTÉ

RÉSUMÉ

Les mécanismes de tenségrité sont progressivement reconnus comme des alternatives potentielles aux mécanismes plus conventionnelles dans le cadre d'applications où la réduction de l'inertie des pièces mobiles et l'augmentation du rapport charge utile sur masse propre sont recherchées. En ce sens, un mécanisme de tenségrité plan à deux degrés de liberté est développé en exploitant une stratégie d'actionnement simple pour assurer que le mécanisme demeure dans des configurations où il peut être prétendu. Des solutions aux problèmes géométriques direct et inverse du mécanisme sont développées et ensuite exploitées pour trouver des expressions analytiques pour les frontières de son espace atteignable.

1. INTRODUCTION

The word *tensegrity* was originally coined by Buckminster Fuller as a combination of the words *tension* and *integrity* [1] after becoming aware of a sculpture created by one of his students, artist Kenneth Snelson [2]. A detailed history of tensegrity systems is provided by Motro [3]. Tensegrity systems (*i.e.* structures or mechanisms) correspond to assemblies of axially loaded components where the nature of each component's loading – tensile or compressive – remains constant for any configuration. This allows the use of cables for the tensile components thus giving these systems the advantage of reduced mass and inertia. Tensegrity systems have a self-stress capability which makes it possible to maintain tension in the cables at all times. However, this is generally only possible in specific configurations, henceforth referred to as *tensegrity configurations*.

Historically, much of the research that has been performed on tensegrity systems has dealt with their use as structures. Among the first to consider the actuation of tensegrity systems by modifying the lengths of their components in order to obtain tensegrity mechanisms were Oppenheim and Williams [4]. Since then, several tensegrity mechanisms have been proposed in the literature, *e.g.* [5]. Some applications that have been considered include a tensegrity flight simulator [6], a tensegrity space telescope [7], a tensegrity force and torque sensor [8], and a tensegrity walking robot [9]. The development of tensegrity mechanisms is motivated by the reduced mass and inertia of their moving parts due to the extensive use of cables. This allows tensegrity mechanisms to be considered as interesting alternatives for high-acceleration applications. Some tensegrity mechanisms also have a deployment capability [10] that, combined with their relatively low weight, makes them attractive for space applications.

As mentioned above, tensegrity mechanisms must be in tensegrity configurations in order for their cables to be prestressed. The determination of these configurations for a given architecture is a challenge that has often been addressed by existing works, a review of which is given in [11]. However, ensuring that a mechanism stays in such configurations as the lengths of its components are being changed is another challenge. In fact, the inherent over-actuation of tensegrity mechanisms requires extremely accurate component length control to maintain acceptable levels of tension in the cables. In past works, the author has curtailed this issue by using extension springs instead of cables for some tensile components [12, 13]. The natural minimization of the potential energy in the mechanism's springs would automatically keep the latter in tensegrity configurations regardless of the lengths of the actuated components. While this represented an elegant solution, the quantities of springs that were used also made the mechanisms deformable when subjected to external loads. In this paper, a new two-degree-of-freedom (2-DoF) planar tensegrity mechanism is developed using a simple hybrid control scheme which allows it to automatically remain in tensegrity configurations. The architecture of the mechanism is described in the next section. Afterwards, its direct kinematic problem (DKP) and inverse kinematic problem (IKP) are solved and the boundaries of its workspace in both the actuator and the Cartesian domain are developed analytically.

2. DESCRIPTION OF MECHANISM ARCHITECTURE

A schematic representation of the mechanism is shown in Fig. 1(a). It is based on Snelson's X-shape tensegrity structure [2] consisting of two compressive components and four tensile components. The compressive components are bars of length L_b that join node pairs A_1A_3 and A_2A_4 while the tensile components are cables joining node pairs A_1A_2, A_2A_3, A_3A_4 and A_1A_4. Revolute joints can be used to make the connections between the components at each node.

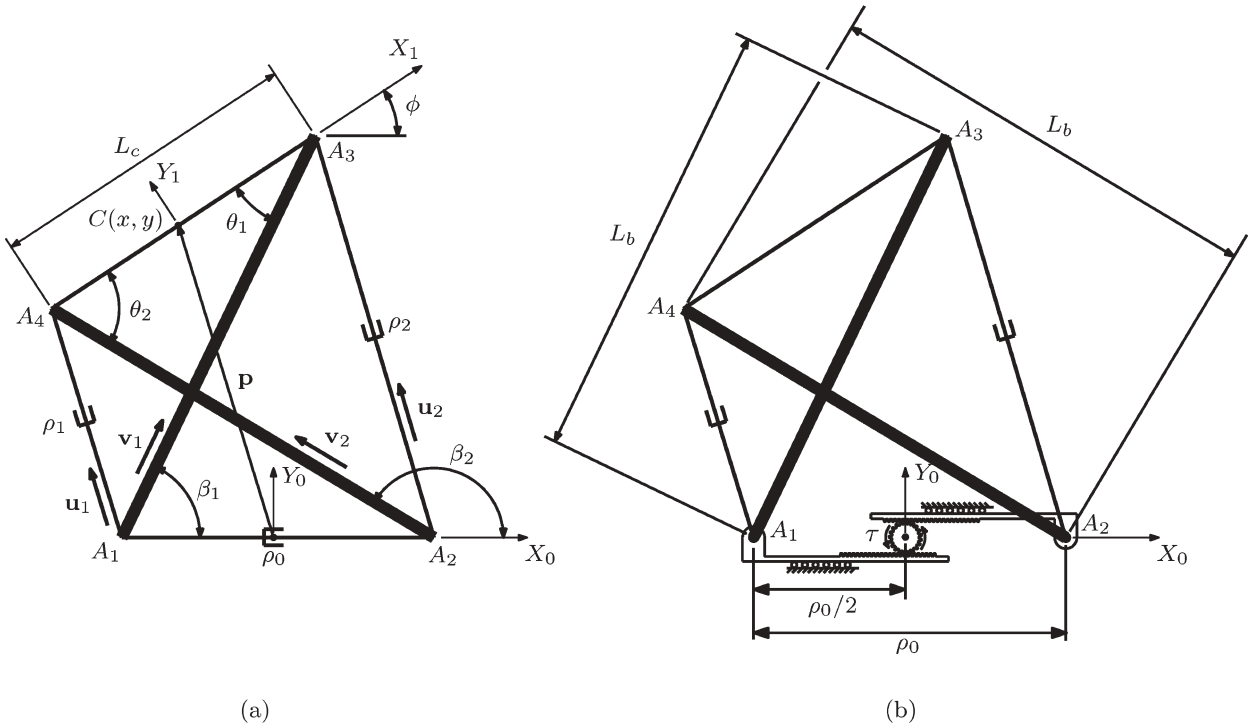

Fig. 1. Schematic diagram of a novel 2-DoF planar tensegrity mechanism.

Alternatively, the inherent flexibility of the cables can be exploited to eliminate the need for revolute joints and thus reduce the overall cost of the mechanism. It can be shown (and can also be seen intuitively) that in order for the mechanism to have self-stress capability with the cables in tension and the bars in compression (*i.e.* a tensegrity configuration) the bars must cross such that their end nodes form a convex quadrilateral. It is noted here that although the bars cross they do not touch each other. This can be achieved, for instance, by creating a slot in one of the bars in which the other bar may slide freely.

The novel aspect of the mechanism is its use of a hybrid actuation scheme that allows it to modify the position of its end-effector while ensuring that it stays in a tensegrity configuration at all times. The actuation scheme consists of a combination of cable length and force control. On one hand, the lengths of the cables joining node pairs A_1A_4 and A_2A_3, represented by ρ_1 and ρ_2, are controlled using motor-driven winches in order to modify the mechanism's configuration. Meanwhile, a constant tensile force f_0 is applied to the cable joining node pair A_1A_2 in order to prestress the mechanism and maintain tension forces in the remaining cables. The length of this last cable is represented by ρ_0. Alternatively, the bottom cable can be replaced by a double rack and pinion mechanism as shown in Fig. 1(b). This allows the mechanism to be attached to ground while maintaining its symmetry and keeping the number of actuators at a minimum. A constant torque τ_0 is applied to the pinion in the counterclockwise direction such that the corresponding forces on the racks (which are constrained to translate on the X_0 axis), directed so as to bring nodes A_1 and A_2 toward each other, is f_0. The combination of length and force control described here has previously been proposed for use with wire-driven mechanisms as a simple method to overcome the required actuation redundancy [14].

A reference frame X_0Y_0 is used to represent the mechanism's base with its origin O located at the centre of the force controlled cable and its X_0 axis parallel to the line passing through nodes

A_1 and A_2. In a similar fashion, a mobile reference frame X_1Y_1 is defined as having its origin C located at the centre of the cable joining nodes A_3 and A_4 and its X_1 axis parallel to the line passing through these nodes. The mobile frame is used to represent the mechanism's end-effector that is chosen to correspond to the cable joining nodes A_3 and A_4 whose length is represented by L_c. As such, the position of the end-effector corresponds to the position of the origin of frame X_1Y_1 expressed in frame X_0Y_0 and given by vector $\mathbf{p} = [x,y]^T$. By modifying ρ_1 and ρ_2 this position can be changed, giving the mechanism its two degrees of freedom. It is noted that the mechanism has two assembly modes that are reflections of themselves about the X_0 axis but only positions of the end-effector with $y \geq 0$ will be considered (without loss of generality).

3. SOLUTION TO THE DIRECT KINEMATIC PROBLEM

The mechanism's DKP is defined as the task of computing the position of its end-effector, given by $\mathbf{p}$ and expressed in the fixed reference frame X_0Y_0, in terms of the known lengths of its length-controlled cables, ρ_1 and ρ_2. It is assumed throughout this paper that a sufficient force is applied to the force-controlled cable to keep all cables in tension regardless of any finite external loads that may be applied to the end-effector. In fact, it is recalled that when the mechanism is in a tensegrity configuration, its level of prestress can be adjusted at will in order to satisfy the above-mentioned condition. In the extreme case, an infinite prestress could be applied such that the tension forces in the cables due to prestress would be infinite and the cables would remain in tension regardless of the finite external force that is applied (clearly, the mechanical limitations of the mechanism's components are not being considered in this model). Referring to Fig. 1(a), unit vectors $\mathbf{v}_1$ and $\mathbf{v}_2$ are defined as being directed along the bars joining node pairs A_1A_3 and A_2A_4 such that

$$[\mathbf{v}_1]_1 = \begin{bmatrix} \cos\theta_1 \\ \sin\theta_1 \end{bmatrix}, \quad [\mathbf{v}_2]_1 = \begin{bmatrix} -\cos\theta_2 \\ \sin\theta_2 \end{bmatrix} \tag{1}$$

where in this section $[\cdot]_i$ represents a vector expressed in frame X_iY_i ($i = 0, 1$). Moreover, it is observed that

$$\cos\theta_j = \frac{L_c^2 + L_b^2 - \rho_j^2}{2L_cL_c} \quad j = 1,2 \tag{2}$$

with $\sin\theta_j = \sqrt{1-\cos^2\theta_j}$ since, in order to remain in a tensegrity configuration with the bars crossing, $0 \leq \theta_j \leq \pi$ must be satisfied at all times. Referring again to Fig. 1(a), the following two vector loop-closure equations can be written

$$[\mathbf{p}]_1 + \frac{L_c}{2}[\mathbf{e}_{X_1}]_1 = \frac{\rho_0}{2}[\mathbf{e}_{X_0}]_1 + L_b[\mathbf{v}_1]_1 \tag{3}$$

$$[\mathbf{p}]_1 + \frac{L_c}{2}[\mathbf{e}_{X_1}]_1 = \frac{\rho_0}{2}[\mathbf{e}_{X_0}]_1 + L_b[\mathbf{v}_2]_1 \tag{4}$$

where $\mathbf{e}_{X_i}$ and $\mathbf{e}_{Y_i}$, are unit vectors in the directions of axes X_i and Y_i, respectively. Summing

these equations and solving for $[\mathbf{p}]_1$ yields

$$[\mathbf{p}]_1 = \frac{L_b}{2}\left([\mathbf{v}_1]_1 + [\mathbf{v}_2]_1\right) \tag{5}$$

With $[\mathbf{v}_1]_1$ and $[\mathbf{v}_2]_1$ being fully defined by Eqs. (1) and (2), the solution to the DKP is obtained as

$$[\mathbf{p}]_0 = \mathbf{Q}[\mathbf{p}]_1$$

where $\mathbf{Q}$ is a rotation matrix bringing frame X_0Y_0 parallel to frame X_1Y_1. An expression for the latter is obtained as

$$\mathbf{Q} = [\,[\mathbf{e}_{X_1}]_0 \quad [\mathbf{e}_{Y_1}]_0\,] = \begin{bmatrix} [\mathbf{e}_{X_0}]_1^T \\ [\mathbf{e}_{Y_0}]_1^T \end{bmatrix} \tag{6}$$

where

$$[\mathbf{e}_{X_0}]_1 = \frac{L_b\left([\mathbf{v}_1]_1 - [\mathbf{v}_2]_1\right) - L_c[\mathbf{e}_{X_1}]_1}{\left\|L_b\left([\mathbf{v}_1]_1 - [\mathbf{v}_2]_1\right) - L_c[\mathbf{e}_{X_1}]_1\right\|} \quad [\mathbf{e}_{Y_0}]_1 = \mathbf{E}[\mathbf{e}_{X_0}]_1 \tag{7}$$

with

$$\mathbf{E} = \begin{bmatrix} 0 & -1 \\ 1 & 0 \end{bmatrix} \tag{8}$$

and where $\|\cdot\|$ denotes the Euclidean norm. Considering only the assembly mode for which $y \geq 0$, the above equation provides a unique solution to the DKP.

4. SOLUTION TO THE INVERSE KINEMATIC PROBLEM

Solving the mechanism's IKP requires the computation of the required cable lengths ρ_1 and ρ_2 for a given end-effector position $\mathbf{p} = [x, y]^T$. Note that all vectors in this section are expressed in the X_0Y_0 frame and so $[\mathbf{p}]_0$ is written as $\mathbf{p}$, etc., in order to alleviate the text. Unit vectors $\mathbf{u}_1$ and $\mathbf{u}_2$ are defined as being directed along the cables joining node pairs A_1A_4 and A_2A_3, respectively. Meanwhile, angles β_1 and β_2 are defined as being measured from the X_0 axis to each of the bars. From Eq. (5), one can write

$$2\mathbf{p} = L_b(\mathbf{v}_1 + \mathbf{v}_2) \tag{9}$$

Isolating the term containing $\mathbf{v}_2$ in the above equation and then squaring both sides yields

$$(2\mathbf{p} - L_b\mathbf{v}_1)^T(2\mathbf{p} - L_b\mathbf{v}_1) = L_b^2 \tag{10}$$

which can be simplified to

$$L_b \mathbf{p}^T \mathbf{v}_1 = \mathbf{p}^T \mathbf{p} \tag{11}$$

where the only unknown is $\mathbf{v}_1$. Knowing that $\mathbf{v}_1 = [\cos\beta_1, \sin\beta_1]^T$ and using the tangent of the half angle substitution with $u = \tan(\beta_1/2)$, Eq. (11) can be rewritten as

$$C_2 u^2 + C_1 u + C_0 = 0 \tag{12}$$

with

$$C_0 = \mathbf{p}^T \mathbf{p} - L_b \mathbf{p}^T \mathbf{e}_1 \tag{13}$$

$$C_1 = -2 L_b \mathbf{p}^T \mathbf{e}_2 \tag{14}$$

$$C_2 = \mathbf{p}^T \mathbf{p} + L_b \mathbf{p}^T \mathbf{e}_1 \tag{15}$$

and where $\mathbf{e_1} = [1,0]^T$ and $\mathbf{e_2} = [0, 1]^T$. The solution for u is found as

$$u = \frac{-C_1 + \delta\sqrt{C_1^2 - 4C_0 C_2}}{2C_2} \tag{16}$$

where $\delta = \pm 1$. This yields a maximum of two solutions for u that translate into two corresponding solutions for β_1 (and $\mathbf{v}_1$). In order to gain some insight into these two solutions, Eq. (9) is represented graphically in Fig. 2 for each of the two solutions (*i.e.* S_1 and S_2). In this figure, the vector sum $L_b(\mathbf{v}_1 + \mathbf{v}_2)$ for each of the two solutions must form a parallelogram of which $2\mathbf{p}$ is a diagonal. It is known that the mechanism's bars must be crossing for it to be in a tensegrity configuration. Furthermore, for practical reasons, only configurations where the X_0

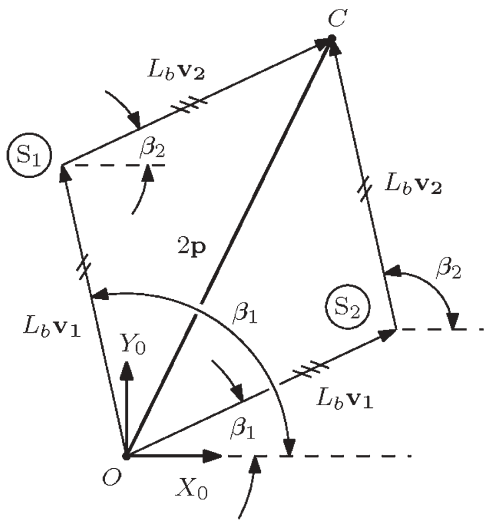

Fig. 2. Graphical representation of the solutions for vectors $\mathbf{v}_1$ and $\mathbf{v}_2$.

coordinates of nodes A_1 and A_2 are non-positive and non-negative, respectively, are to be considered. With this in mind, it can be observed from Fig. 2 that $\beta_2 \geq \beta_1$ must always be satisfied which can only occur for solution S_2. Looking back at Eq. (16), only one of the two solutions for u (and equivalently for $\mathbf{v}_1$) is valid. This solution can be shown to correspond to $\delta = -1$. Given now the solution for $\mathbf{v}_1$, Eq. (9) can easily be solved for $\mathbf{v}_2$.

With $\mathbf{v}_1$ now known, Eq. (3) is used to solve for ρ_0. The equation is first rewritten in order to isolate $\mathbf{e}_{\mathbf{X}_1}$

$$\mathbf{p} - L_b\mathbf{v}_1 + \frac{\rho_0}{2}\mathbf{e}_{\mathbf{X}_0} = \frac{L_c}{2}\mathbf{e}_{\mathbf{X}_1} \tag{17}$$

where all vectors are now expressed in the X_0Y_0 frame. Squaring this expression generates the following quadratic equation

$$D_2\rho_0^2 + D_1\rho_0 + D_0 = 0 \tag{18}$$

where the coefficients are

$$D_0 = (\mathbf{p} - L_b\mathbf{v}_1)^T(\mathbf{p} - L_b\mathbf{v}_1) - \frac{L_c^2}{4} \tag{19}$$

$$D_1 = (\mathbf{p} - L_b\mathbf{v}_1)^T\mathbf{e}_{\mathbf{X}_0} \tag{20}$$

$$D_2 = \frac{1}{4} \tag{21}$$

In the general case, this will yield two solutions for ρ_0. These solutions can be visualized in Fig. 3 where only the bars and the end-effector cable are shown. In this figure, the connection at node A_3 between the end-effector cable and the bar joining nodes A_1 and A_3 has been temporarily removed and the orientations of the bars have been constrained since $\mathbf{v}_1$ and $\mathbf{v}_2$ are

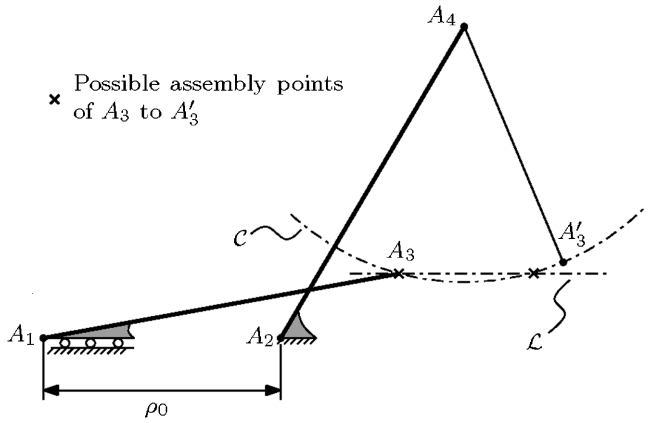

Fig. 3. Graphical representation of the two solutions for ρ_0.

known. Furthermore, it has been assumed for simplicity that the position of node A_2 is fixed while that of node A_1 is free to translate along the horizontal (*i.e.* X_0 axis). As such, when ρ_0 is varied, node A_3 is displaced along line $\mathcal{L}$. Meanwhile, as the end-effector cable is rotated about node A_4, node A'_3 moves about a circle $\mathcal{C}$ of radius L_c centred at node A_4. It follows that solving Eq. (18) corresponds to finding the intersections between a line and a circle which has a maximum of two solutions. Furthermore, these two solutions are physically possible for some positions of the end-effector. Finally, the lengths of the length-actuated cables can be found by writing the following two vector loop-closure equations

$$\rho_1 \mathbf{u}_1 = \rho_0 \mathbf{e}_{\mathbf{X}_0} + L_b \mathbf{v}_2 \tag{22}$$

$$\rho_2 \mathbf{u}_2 = -\rho_0 \mathbf{e}_{\mathbf{X}_0} + L_b \mathbf{v}_1 \tag{23}$$

Squaring both sides of these two equations, simplifying and then taking the square root yields

$$\rho_1 = \sqrt{(\rho_0 \mathbf{e}_{\mathbf{X}_0} + L_b \mathbf{v}_2)^T (\rho_0 \mathbf{e}_{\mathbf{X}_0} + L_b \mathbf{v}_2)} \tag{24}$$

$$\rho_2 = \sqrt{(-\rho_0 \mathbf{e}_{\mathbf{X}_0} + L_b \mathbf{v}_1)^T (-\rho_0 \mathbf{e}_{\mathbf{X}_0} + L_b \mathbf{v}_1)} \tag{25}$$

which is the sought solution to the mechanism's IKP. Since it has been established that a single solution exists for both $\mathbf{v}_1$ and $\mathbf{v}_2$ while two solutions exist for ρ_0, the IKP has a maximum of two possible solutions. The choice between these two solutions of the IKP, when they exist, will be discussed in greater detail in section 5.2.

5. DETERMINATION OF THE WORKSPACE BOUNDARIES

The mechanism's workspace is defined here as the set of all configurations that are attainable by the mechanism while remaining in a tensegrity configuration. In tensegrity configurations, the level of prestress in the mechanism can be adjusted freely by changing the tension f_0 in the force controlled cable. It follows that, regardless of the external or inertial loads that might be acting on the mechanism, f_0 can be adjusted such that tension is maintained in all of the cables. This of course assumes that there is no mechanical limit to the loads capable of being sustained by the mechanism's components. In what follows, for practical reasons, the mechanism's workspace will be limited to configurations where node A_1 (A_2) has a negative (positive) X_0 coordinate.

The conditions needing to be satisfied for the mechanism to be in a tensegrity configuration will now be exploited to determine its workspace boundaries. It is recalled that the mechanism's tensegrity configurations are those where the bars cross such that their end nodes form a convex quadrilateral. Assuming that the mechanism is initially in a tensegrity configuration, it can be observed that it will stay in such a configuration as long as no subset of three of its four nodes become collinear. While this implicitly requires the mechanism's components to maintain nonzero lengths, the case where $\rho_0 = 0$ will be looked at separately since, as will be seen, it leads to its own workspace boundary. The following list of situations that lead to potential workspace boundaries can thus be generated:

I. $\rho_0 = 0$.
II. Nodes A_1, A_2 and A_3 are collinear.
III. Nodes A_1, A_2 and A_4 are collinear.
IV. Nodes A_2, A_3 and A_4 are collinear.
V. Nodes A_1, A_3 and A_4 are collinear.

In addition, the meet of the two solutions to the mechanism's IKP can also correspond to a workspace boundary. The following item is thus added to the above list:

VI. Meet of the IKP's two solutions.

In the following sections, each of these situations will be translated to geometric entities in both the actuator and Cartesian spaces. The situations where $L_b > L_c$, $L_b = L_c$ and $L_b < L_c$ must be considered separately. However, in order to alleviate the text, only the case where $L_b > L_c$ will be presented. This represents the most common scenario for the given mechanism architecture. Results for the other two cases have been found using a similar approach.

5.1. Actuator Workspace

I. $\rho_0 = 0$.

Looking at Fig. 1(a), it is observed that nodes A_1 and A_2 are coincident when $\rho_0 = 0$. This is only possible when

$$\mathcal{C}_1 : \rho_1 = \rho_2 = L_b \tag{26}$$

which defines a point in the actuator space.

II. Nodes A_1, A_2 and A_3 are collinear.

Referring once again to Fig. 1(a), nodes A_1, A_2 and A_3 will be collinear only when $\beta_1 = 0$ or π which translates to

$$\cos\beta_1 = \frac{L_b^2 + \rho_0^2 - \rho_2^2}{2L_b\rho_0} = \pm 1 \tag{27}$$

Squaring both sides of this equation and rearranging, one finds:

$$\frac{(L_b + \rho_0 - \rho_2)(L_b + \rho_0 + \rho_2)(L_b - \rho_0 - \rho_2)(L_b - \rho_0 + \rho_2)}{4L_b^2\rho_0^2} = 0 \tag{28}$$

Knowing that $L_b > 0$ and assuming $\rho_0 > 0$ (the case where $\rho_0 = 0$ has already been considered), this leads to the following four conditions

II-i. $L_b + \rho_0 - \rho_2 = 0$ II-ii. $L_b + \rho_0 + \rho_2 = 0$
II-iii. $L_b - \rho_0 - \rho_2 = 0$ II-iv. $L_b - \rho_0 + \rho_2 = 0$

of which II-ii can never be satisfied since component lengths cannot be negative. When looking to satisfy these conditions, one is interested only in those mechanism configurations where a static equilibrium is possible with the cables in tension and the bars in compression. Taking this into account, condition II-i is satisfied only when $\beta_1 = \beta_2 = \pi$ as illustrated schematically in Fig. 4(a). From this figure, condition II-i can be seen to correspond to the following point in the

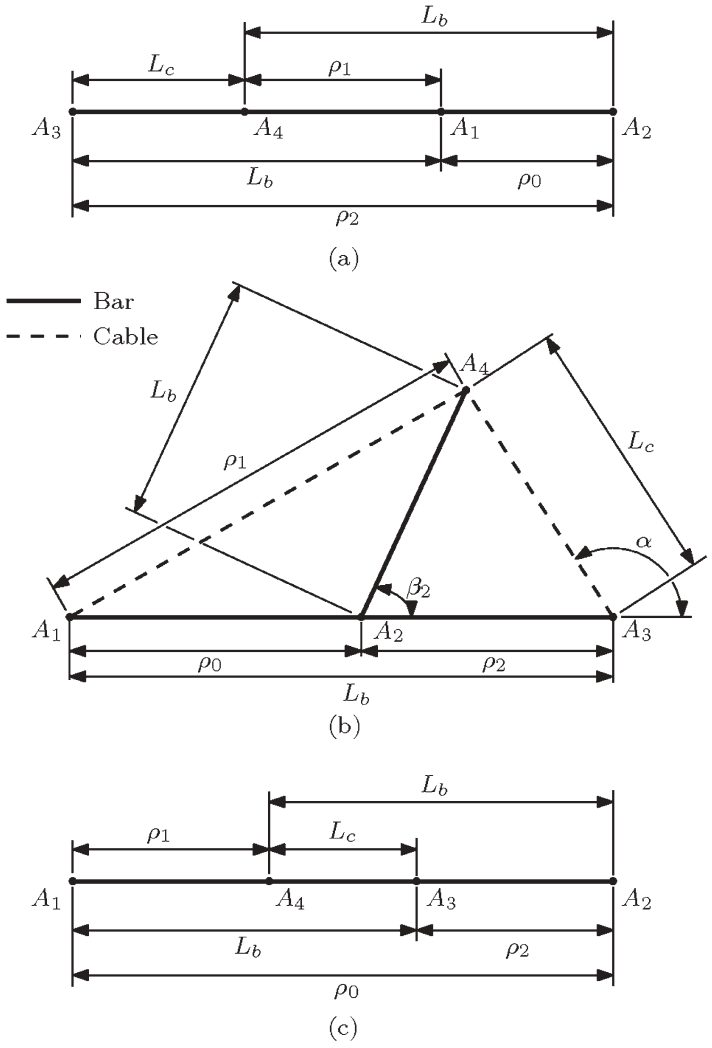

Fig. 4. Geometrical representation of condition II: a) II-i, b) II-iii, c) II-iv.

actuator space

$$\mathcal{C}_2 : \rho_1 = L_b - L_c \ , \ \rho_2 = L_b + L_c \tag{29}$$

Turning now to condition II-iii, it can be seen to be satisfied only for configurations where $\beta_1 = 0$. This is shown in Fig. 4(b) where the bar joining node pair A_2A_4 remains free to pivot about node A_2 as ρ_1 and ρ_2 are modified. From this figure, one has

$$\cos\beta_2 = \frac{\rho_2^2 + L_b^2 - L_c^2}{2\rho_2 L_b} = -\frac{\rho_0^2 + L_b^2 - \rho_1^2}{2\rho_0 L_b} \tag{30}$$

Substituting $\rho_0 = L_b - \rho_2$ into this equation and simplifying leads to

$$-\frac{\rho_1^2\rho_2 + L_b\rho_2^2 - (L_b^2 + L_c^2)\rho_2 + L_b(L_c^2 - L_b^2)}{2L_b\rho_2(L_b - \rho_2)} = 0 \tag{31}$$

where the denominator is equal to zero only when $\rho_0 = 0$ or $\rho_2 = 0$ (these situations are considered elsewhere). The actuator space curve corresponding to this condition is thus

$$\mathcal{C}_3 : \rho_1^2\rho_2 + L_b\rho_2^2 - \left(L_b^2 + L_c^2\right)\rho_2 + L_b\left(L_c^2 - L_b^2\right) = 0 \tag{32}$$

Finally, condition II-iv can be satisfied only when $\beta_1 = 0$ and $\beta_2 = \pi$ as shown in Fig. 4(c). This can be seen to correspond to the following point in the actuator space

$$\mathcal{C}_4 : \rho_1 = \rho_2 = L_b - L_c \tag{33}$$

III. Nodes A_1, A_2 and A_4 are collinear.

Due to the mechanism's inherent symmetry, situation III is equivalent to situation II where ρ_1 and ρ_2 are simply interchanged. In this way, based on developments similar to those given for situation II, situation III leads to the following additional geometric entities in the actuator space

$$\mathcal{C}_5 : \rho_1 = L_b + L_c \ , \ \rho_2 = L_b - L_c \tag{34}$$

$$\mathcal{C}_6 : \rho_1\rho_2^2 + L_b\rho_1^2 - \left(L_b^2 + L_c^2\right)\rho_1 + L_b\left(L_c^2 - L_b^2\right) = 0 \tag{35}$$

where it is noted that situation III also leads to $\mathcal{C}_4$.

IV. Nodes A_2, A_3 and A_4 are collinear.

Referring to Fig. 1(a), nodes A_2, A_3 and A_4 are collinear when $\theta_2 = 0$ or π or when

$$\cos\theta_2 = \frac{L_b^2 + L_c^2 - \rho_2^2}{2L_bL_c} = \pm 1 \tag{36}$$

Squaring both sides of this equation and rearranging yields

$$\frac{(L_b + L_c - \rho_2)(L_b + L_c + \rho_2)(L_b - L_c + \rho_2)(L_b - L_c - \rho_2)}{4L_b^2L_c^2} = 0 \tag{37}$$

which leads to the following four conditions

IV-i. $L_b + L_c - \rho_2 = 0$ IV-ii. $L_b + L_c + \rho_2 = 0$

IV-iii. $L_b - L_c + \rho_2 = 0$ IV-iv. $L_b - L_c - \rho_2 = 0$

of which IV-ii can never be satisfied since component lengths cannot be negative. Moreover, IV-iii cannot be satisfied based on the fact that $L_b > L_c$ (which is the case being considered). Looking now at condition IV-i, it can be seen to be satisfied only when $\beta_1 = \beta_2 = \pi$, a configuration which has already been shown in Fig. 4(a). It follows that conditions IV-i and II-i are equivalent and, as such, condition IV-i corresponds to the point in the actuator space defined in Eq. (29) as $\mathcal{C}_2$. Condition IV-iv, for its part, is satisfied only when $\theta_2 = 0$ which leads to configurations such as the one shown in Fig. 5 where node A_3 is located along the line defined

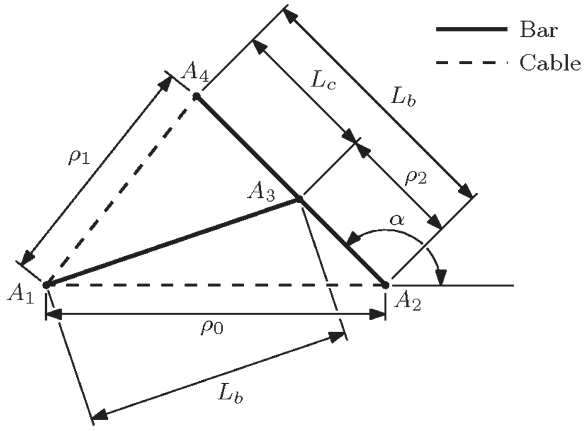

Fig. 5. Geometrical representation of condition IV-iv.

by nodes A_2 and A_4. The geometric entity corresponding to IV-iv is simply found from the definition of the condition as

$$\mathcal{C}_7 : \rho_2 = L_b - L_c \tag{38}$$

V. Nodes A_1, A_3 and A_4 are collinear.

Again, due to the mechanism's symmetry, situation V is analogous to situation IV where ρ_1 and ρ_2 are interchanged thus leading to the following additional geometric entity in the actuator space

$$\mathcal{C}_8 : \rho_1 = L_b - L_c \tag{39}$$

VI. Meet of the IKP's two solutions.

It was shown in section 4 that there are two possible solutions to the mechanism's IKP. These originate from the two solutions of the quadratic polynomial given in Eq. (18). Situations where the two solutions of the IKP meet are of interest since they represent potential workspace boundaries. From Eq. (18), the meet of the IKP's solutions is seen to correspond to situations where

$$\Delta = D_1^2 - 4D_0D_2 = 0 \tag{40}$$

Substituting Eqs. (19)–(21) in the above equation yields

$$\Delta = -\frac{1}{4}\left(2y - 2L_b v_{1_y} - L_c\right)\left(2y - 2L_b v_{1_y} + L_c\right) = 0 \tag{41}$$

where v_{1_y} is the Y_0 component of vector $\mathbf{v}_1$. Referring to Fig. 1(a), one can observe that

$$v_{1_y} = \sin\beta_1 = \frac{1}{L_b}\left(y + \frac{L_c}{2}\sin\phi\right) \tag{42}$$

Substituting this result in Eq. (41) and simplifying leads to

$$\Delta = \frac{L_c^2 \cos^2\phi}{2} = 0 \tag{43}$$

where it becomes clear that the meet of the IKP's two solutions corresponds to situations where $\phi = \pm\pi/2$. This result can be interpreted geometrically from Fig. 3 where a vertical end-effector cable implies that circle $\mathcal{C}$ and line $\mathcal{L}$ are tangent thus leading to a double root of Eq. (18). Looking now at Fig. 1(a), it is observed that when $\phi = \pm\pi/2$ one has

$$\rho_0 - L_b(\cos\theta_1 + \cos\theta_2) = 0 \tag{44}$$

Substituting Eq. (2) in the above yields

$$\frac{1}{2\rho_0}\left(\rho_1^2 + \rho_2^2 - 2L_b^2\right) = 0 \tag{45}$$

from which the curve in the actuator space corresponding to the meet of the IKP's solutions is found as

$$\mathcal{C}_9 : \rho_1^2 + \rho_2^2 - 2L_b^2 = 0 \tag{46}$$

The mechanism's actuator workspace is finally obtained by plotting the geometric entities $\mathcal{C}k$ (k = 1,2, …,9). in the two-dimensional actuator space as shown in Fig. 6. It can be seen that the actuator workspace is divided into three regions denoted as $\mathcal{R}_1$, $\mathcal{R}_2$ and $\mathcal{R}_3$. The dividing boundaries of these regions are the curves corresponding to the meet of two solutions to the mechanism's IKP.

5.2. Cartesian Workspace

The mechanism's Cartesian workspace is found by mapping the geometrical entities listed in the previous section to the Cartesian space. $\mathcal{C}_1$ corresponds to situations where $\rho_0 = 0$. In this case, nodes A_1 and A_2, which are coincident, form an isosceles triangle with nodes A_3 and A_4

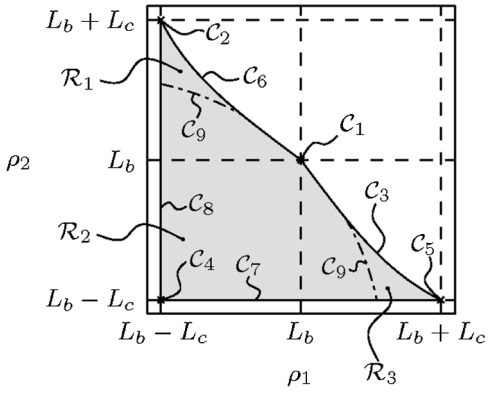

Fig. 6. Actuator workspace when $L_b > L_c$.

where two sides are of length L_b and the other of length L_c (see Fig. 1a). Moreover, the entire mechanism is free to pivot about nodes A_1 and A_2. As this occurs, the end-effector reference point C moves about the following circle

$$\mathcal{C}_1 : x^2 + y^2 = L_b^2 - \frac{L_c^2}{4} \tag{47}$$

which is a potential boundary of the Cartesian workspace. Referring now to Fig. 4(a), $\mathcal{C}_2$ can be observed to be mapped to the following point in the Cartesian space

$$\mathcal{C}_2 : x = -L_b \, , \, y = 0 \tag{48}$$

In order to map $\mathcal{C}_3$ to Cartesian space, one can observe from Fig. 4(b) that node C is constrained to a circle of radius $L_c/2$ centred at $x_0 = L_b - \rho_0/2$ and $y_0 = 0$. A parametric representation of this circle in terms of angle α (defined in Fig. 4b) is obtained as

$$\mathcal{C}_3 : x = L_b - \frac{\rho_0}{2} + L_c \cos\alpha, \quad y = L_c \sin\alpha \tag{49}$$

An expression for ρ_0 in terms of α is found by substituting $\rho_2 = L_b - \rho_0$ into the following expression

$$\cos\alpha = \frac{L_b^2 - L_c^2 - \rho_2^2}{2L_c\rho_2} \tag{50}$$

and then solving for ρ_0 which leads to

$$\rho_0 = L_b + L_c \cos\alpha \pm \sqrt{L_b^2 - L_c^2 \sin^2\alpha} \tag{51}$$

where it is that found the useful portion of the parametric curve (in terms of the Cartesian workspace) corresponds to the negative sign for the square root. As far as $\mathcal{C}_4$ is concerned, it can be observed from Fig. 4(c) that it corresponds to

$$\mathcal{C}_4 : x = y = 0 \tag{52}$$

Due to the mechanism's symmetry about the Y_0 axis, Cartesian space equivalents to $\mathcal{C}_5$ and $\mathcal{C}_6$ can be found simply from $\mathcal{C}_2$ and $\mathcal{C}_3$ as

$$\mathcal{C}_5 : x = L_b \, , \, y = 0 \tag{53}$$

$$\mathcal{C}_6 : x = -L_b + \frac{\rho_0}{2} - L_c \cos\alpha, \quad y = L_c \sin\alpha \tag{54}$$

where, for $\mathcal{C}_6$, ρ_0 is once again given by Eq. (51). Looking now at the mapping of $\mathcal{C}_7$ to Cartesian space, it can be seen in Fig. 5 that the end-effector's position is constrained to a circle of radius $L_b - L_c/2$ centred at $x_0 = \rho_0/2$ and $y_0 = 0$. This is represented parametrically in terms of

angle α as

$$\mathcal{C}_7 : x = \frac{\rho_0}{2} + \left(L_b - \frac{L_c}{2}\right)\cos\alpha \ , \ y = \left(L_b - \frac{L_c}{2}\right)\sin\alpha \tag{55}$$

An equation for ρ_0 in terms of α is found by substituting $\rho_2 = L_b - L_c$ into the following expression for the cosine of α (refer to Fig. 5)

$$\cos\alpha = \frac{L_b^2 - \rho_2^2 - \rho_0^2}{2\rho_2\rho_0} \tag{56}$$

and then solving for ρ_0 which leads to

$$\rho_0 = (L_c - L_b)\cos\alpha \pm \sqrt{2L_bL_c\sin^2\alpha + (L_b^2 + L_c^2)\cos^2\alpha - L_c^2} \tag{57}$$

where the useful portion of the curve is found to correspond to the positive square root. Once again exploiting the mechanism's symmetry, the mapping of $\mathcal{C}_8$ to Cartesian space is obtained as

$$\mathcal{C}_8 : x = -\frac{\rho_0}{2} - \left(L_b - \frac{L_c}{2}\right)\cos\alpha \ , \ y = \left(L_b - \frac{L_c}{2}\right)\sin\alpha \tag{58}$$

with ρ_0 once again given by Eq. (57). Moving on to $\mathcal{C}_9$, its Cartesian mapping is first obtained by solving Eq. (3) for $\mathbf{p}$ as follows

$$\mathbf{p} = -\frac{\rho_0}{2}\mathbf{e}_{\mathbf{X}_0} + L_b\mathbf{v}_1 - \frac{L_c}{2}\mathbf{e}_{\mathbf{X}_1} \tag{59}$$

Knowing that $\mathbf{e}_{\mathbf{X}_0} = [1,0]^T$, $\mathbf{v}_1 = [\cos\beta_1, \sin\beta_1]^T$ and $\mathbf{e}_{\mathbf{X}_1} = [\cos\phi, \sin\phi]^T$ and noting that $\phi = \pm\pi/2$ for the case under study, parametric expressions for the end-effector's position in terms of β_1 can be found as

$$\mathcal{C}_9 : x = -\frac{\rho_0}{2} + L_b\cos\beta_1 \ , \ y = -\frac{L_c}{2} + L_b\sin\beta_1 \tag{60}$$

where an expression for ρ_0 in terms of β_1 must still be found. Subtracting Eq. (4) from Eq. (3), substituting for $\mathbf{e}_{\mathbf{X}_0}$, $\mathbf{v}_1$ and $\mathbf{e}_{\mathbf{X}_1}$ with the expressions given above and rearranging, one obtains

$$L_b\sin\beta_1 - L_c = L_b\sin\beta_2 \tag{61}$$

$$L_b\cos\beta_1 - \rho_0 = L_b\cos\beta_2 \tag{62}$$

Squaring both of these equations, adding them together and solving for ρ_0 yields

$$\rho_0 = L_b\cos\beta_1 \pm \sqrt{L_b^2\cos^2\beta_1 + 2L_bL_c\sin\beta_1 - L_c^2} \tag{63}$$

Having now mapped each actuator workspace boundary to the Cartesian space, the Cartesian workspace can be plotted as shown in Fig. 7. In the previous section, the actuator workspace was seen to be divided into three regions. The areas of the Cartesian workspace that correspond to these regions are shown in Fig. 7. It can be observed that regions $\mathcal{R}_1$ and $\mathcal{R}_3$ both overlap respective portions of region $\mathcal{R}_2$. It is important to note that the mechanism's IKP has multiple solutions only in these overlapping areas of the Cartesian workspace. In such cases, one of the solutions corresponds to a point in the $\mathcal{R}_2$ region of the actuator space while the other belongs to either the $\mathcal{R}_1$ or $\mathcal{R}_3$ region (see Fig. 6). In these areas of the Cartesian workspace, either of the solutions to the IKP can be used with the choice between solutions being motivated by, for instance, the mechanism's performance (*e.g.* its stiffness). However, it must be understood that changing from one solution of the IKP to the other requires the mechanism to pass through the $\mathcal{C}_9$ curve. While this is not an issue per se (*i.e.* the mechanism is not singular and its behaviour does not otherwise change in configurations corresponding to the $\mathcal{C}_9$ curve), the need to traverse $\mathcal{C}_9$ in order to change from one IKP solution to another adds a constraint to the trajectory that is followed in Cartesian space. Finally, it should be remarked that with the exception of $\mathcal{C}_9$, the mechanism should never be positioned on the workspace boundaries as it becomes unstable (*i.e.* it loses the ability to withstand arbitrary external loads with the cables remaining in tension). It follows that the mechanism's workspace is an open set both in the actuator and Cartesian spaces.

6. CONCLUSION

A novel 2-DoF planar tensegrity mechanism that uses a simple actuation scheme to ensure it always remains in tensegrity configurations was presented. Whereas mechanisms with such capabilities have been developed in the past, they have often relied on the use of springs to achieve the same objectives (which either requires the realization of zero rest length springs or leads to reductions in the mechanism's workspace size). A complete kinematic analysis of the mechanism was performed using a geometrically-inspired approach. The mechanism was found to have only one solution of interest to its direct kinematic problem while two valid solutions exist to its inverse kinematic problem. The mechanism's workspace boundaries were also computed analytically. Although the mechanism studied in this work is quite simple and of limited use, it has provided significant insight into some of the issues associated with tensegrity mechanisms. Work on the mechanism's stiffness analysis is currently ongoing. Future research

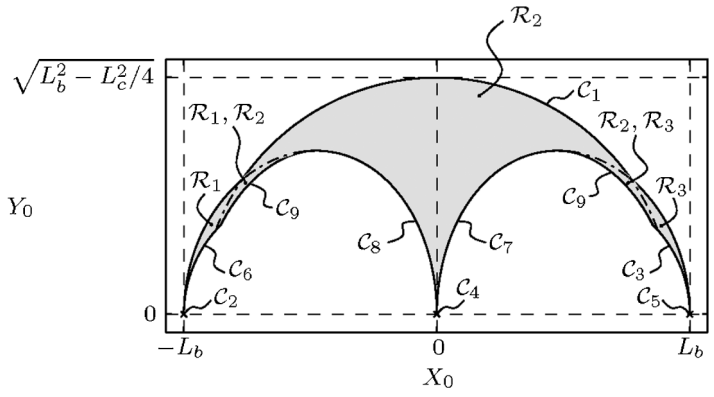

Fig. 7. Cartesian workspace when $L_b > L_c$.

should deal with the development of spatial tensegrity mechanisms based on the principles outlined in this paper.

ACKNOWLEDGEMENT

The author wishes to thank the Natural Sciences and Engineering Research Council of Canada (NSERC) for its financial support.

REFERENCES

1. Fuller, B., "*Tensile-integrity structures,*" United States Patent No. 3,063,521, November 13, 1962.
2. Snelson, K., "*Continuous tension, discontinuous compression structures,*" United States Patent No. 3,169,611, February 16, 1965.
3. Motro, R., "Tensegrity systems: The state of the art," *International Journal of Space Structures*, Vol. 7, No. 2, pp. 75–83, 1992.
4. Oppenheim, I.J. and Williams, W.O., "Tensegrity prisms as adaptive structures," *ASME Adaptive Structures and Material Systems*, Vol. 54, pp. 113–120, 1997.
5. Marshall, M. and Crane, C.D., III., "Design and analysis of a hybrid parallel platform that incorporates tensegrity," in *Proceedings of the ASME 2004 Design Engineering Technical Conferences and Computers and Information in Engineering Conference*, Salt Lake City, Utah, U.S.A., pp. 535–540, 2004.
6. Sultan, C. and Corless, M., "Tensegrity flight simulator," *Journal of Guidance, Control, and Dynamics*, Vol. 23, No. 6, pp. 1055–1064, 2000.
7. Sultan, C., Corless, M. and Skelton, R.E., "Peak to peak control of an adaptive tensegrity space telescope," in *Proceedings of the International Society for Optical Engineering*, Vol. 3667, pp. 190–201, 1999.
8. Sultan, C. and Skelton, R., "A force and torque tensegrity sensor," *Sensors and Actuators, A: Physical*, Vol. 112, No. 2–3, pp. 220–231, 2004.
9. Paul, C., Lipson, H. and Valero-Cuevas, F., "Design and control of tensegrity robots for locomotion," *IEEE Transactions on Robotics*, Vol. 22, No. 5, pp. 944–957, 2006.
10. Sultan, C. and Skelton, R.E., "Tendon control deployment of tensegrity structures," in *Proceedings of the SPIE- The International Society for Optical Engineering*, Vol. 3323, pp. 455–466, 1998.
11. Tibert, A.G. and Pellegrino, S., "Review of form-finding methods for tensegrity structures," *International Journal of Space Structures*, Vol. 18, No. 4, pp. 209–223, 2003.
12. Arsenault, M. and Gosselin, C., "Kinematic and static analysis of a three-degree-of-freedom spatial modular tensegrity mechanism," *International Journal of Robotics Research*, Vol. 27, No. 8, pp. 951–966, 2008.
13. Arsenault, M. and Gosselin, C., "Kinematic and static analysis of a 3-PUPS spatial tensegrity mechanism," *Mechanism and Machine Theory*, Vol. 44, No. 1, pp. 162–179, 2009.
14. Bouchard, S. and Gosselin, C., "A simple control strategy for overconstrained parallel cable mechanisms," in *Proceedings of the 20th Canadian Congress of Applied Mechanics (CANCAM)*, Montréal, Québec, Canada, 2005.